Dynamic modeling of spinal electromyographic activity during various conditions [1]

E. A. Jonckheere and P. Lohsoonthorn
Dept. of Electrical Engineering–Systems
University of Southern california
Los Angeles, CA 90089-2563

R. Boone
PRP Entreprises
Auckland 1309, New Zealand

Abstract

The surface Electromyographic (sEMG) signals recorded along the spine during a rocking motion created by feedback coupling between the motion of the spine and the efferent nerve fibers at the dural attachment points are giving various linear dynamical models of the ARIMA type. The most significant dynamical phenomenon is the nonlinear switching among the various linear models. The switchings represent transitions among qualitatively different modes of the motion of the spine, referred to as Levels 1, 2, 3. Statistical analysis reveals a definite relationship between the qualitatively assessed levels and the various quantitatively relevant models. Finally, it is shown that the higher the level of care, the more reliable the model, that is, the better the model is able to predict the motion as specified by the sEMG signal.

1 Introduction

In a book [2] that has attracted a fair amount of attention, the Scandinavian neurosurgeon Alf Breig introduced the concept of "adverse mechanical cord tension" in the central nervous system. The tenet of this theory is the fact that the dura mater of the spinal cord is attached to the bony vertebrae at the cervical and sacral regions, and, consequently, vertebral misalignment can create pathological tension patterns within the spinal cord, itself impairing nerve function. To be anatomically more specific, the meninges attach to the foramen magnum, pass though the ring of the atlas and insert in strips to the second and third cervical vertebrae, and in smaller strips to the fourth through seventh segments, and again at the sacrum and coccyx through the filum terminale. In another slightly different theory, it is the dentate ligaments rather than the dural attachments that transmit tension to the spinal cord. The dentate ligament hangs the cord to the foramen magnum and the cervical vertebrae via its attachment to the dura, so that excessive loads on the midbrain, pons, and medulla are avoided. However, in biomechanical pathological conditions the dentate ligament can have the adverse effect of inducing adverse mechanical cord tension. Alf Breig stated that, although the dentate ligaments transmit tension, by far the greater tension is produced by factor of body posture and by the nature of the dural attachments at the foramen magum and the filum terminale. Tension in the cord can promote hyperstimulation of the proprioceptive afferent fibers resulting in impaired function of the spine and other areas of the central nervous system. It has been argued by Breig that some diseases have this biomechanical origin and that relief of adverse mechanical cord tension could eliminate these diseases [3].

More closely related to the present paper is the fact that dural attachments create a coupling between the biomechanics of the spine and the central nervous system. More specifically, dural attachments appear to create a feedback from the mechanical movement of the spine to the electrical activity of efferent nerve fibers. That some feedback occurs has been demonstrated by a form of health care known as Network Spinal Analysis (NSA). In this form of health care, the NSA practitioner (at this time all chiropractors) locates specific manual contact points based on their professional assessment of the status of the active, passive, and neural subsystems supporting the normal function of the nervous system[9]. After a period of time, the nervous system becomes entrained to the point where the contacts elicit an oscillation that takes the form of a spontaneous involuntarly controlled rocking motion of the musculature of the spine. This is referred to as "wave." Although the recipient can voluntarily stop this movement, the wave produces a rather intensive exercise for the spine and back musculature that is not reproducible by any other physicotherapeutical means. The latter fact is confirmed by asking the patient to fake the wave motion and observing that the sEMG signals generated have far lower intensity and a completely different waveform compared to the spontaneous involuntary wave motion.

It takes some time before the recipients of NSA are able to experience this motion in its full manifestation. The learning or "entrainment" process is characterized by three Levels of care. The level of care 1 through 3 is numbered in association with the number of anticipated rhythmically entrained spinal oscillators. In level 1, the spinal segment contacted is entrained to the respiratory rhythm, at least visually. This is the early onset period, during which the wave motion is restricted to small localized movements. In level 2, two spinal (coupled) oscillators engage, in the vertebral-dural relationship areas or in the immediate vicin-

ity of those. At this stage, gentle rocking motion become more precise. In Level 3 of care, the two spinal oscillators already developed in level 2, such as occiput and sacrum, are still entrained, in addition to the development of a third thoracic-sternal oscillator. This level has very specific movements of the spine and highly coordinated with the deep breathing patterns.

Retrospective study demonstrates that recipients of this form of care experience health and restorative benefits. As well, other research has also shown therapeutic benefits for a quadraplegic patient five years post injury when subjected to involuntary physical activity [8].

In regard to NSA the recorded sEMG signals take the form of a "background" signal interrupted by "bursts" of accrued sEMG activity [1], the frequency and intensity of which increase with the Level of care. In this paper we look at the signal-theoretic and dynamic properties of the sEMG signals generated during the process of entraining patients from Level 1 to Level 3. The goal was to provide some objective mathematical confirmation of the transition between the Levels of care, which so far have been left to the practitioner's subjective judgment and physical assessments. To achieve this task, we developed "black box" dynamical models of the ARIMA type for the various segments of the data record. Each segment corresponded to a Level of care as well as the recipient's position (sitting, prone, supine). Our objective was to establish that the models are "Level specific" and "position specific" and that there is an identifiable trend in the dynamical models of the signals generated from one Level to the next. More specifically, it was shown that the various Levels could be distinguished by the predictability of the sEMG signals as the error between the signal and its dynamical prediction decreases with the Level of care.

2 Data collection protocol

The sEMG signals from the muscle groups lateral to the spine were recorded by means of noninvasive electrodes placed at the cervical, thoracic, lumbar and sacral regions with the recipient of NSA care successively in the prone, sitting, and supine positions. The electrodes were inputs to an Insight Millenium sEMG machine. While this machine allows for such preprocessing as low pass filtering, we used the raw sEMG data. The analog output signals of the amplifiers were themselves inputs to a Measurement Computing DAS16/16 converter board with the sampling rate set to 4000 samples/sec.

In this study, a recipient of NSA care, who was assessed to be in Level 3, was taken progressively from early Level 1 to advanced Level 3. There were four readings shown in chronological order with the corresponding Levels and positions in Table 1.

recording	segment (model)	level	position
1	1,2,3	1,2	prone
2	4,5,6	2,3	prone
3	7,8,9	2	sitting
4	10,11,12	3	supine

Table 1: Various recording at various levels in various positions.

There were short rest periods between consecutive recordings, during which the recipient was put in another position and the data collection software reinitialized. Each recording had four channels (cervical, thoracic, lumbar and sacral). Each channel recording consisted of 196,608 data points (49 seconds). In this paper we focus on the cervical signal. Each of the 4 cervical recordings was divided into 3 segments of 65,536 samples (16 secs/segment). The long range cervical signal was hence decomposed into 12 segments. Each segment was meant to be representative of a Level of care (1, 2 or 3) together with a position (prone, sitting, supine).

3 ARIMA modeling

3.1 theoretical overview
An *Auto Regressive Integrated Moving Average* $ARIMA(p, d, q)$ model of a nonstationary experimentally observed time series $\{y(k)\}$ is

$$AR_p(L)\left((1 - L)^d y(k)\right) = MA_q(L)\epsilon(k) \qquad (1)$$

where AR_p and MA_q are the autoregressive and moving average polynomials of degree p, q, respectively, in the delay operator $L(= z^{-1})$, with the z-roots of AR_p inside the unit disk, $d \geq 0$ is the order of integration, and ϵ is an uncorrelated sequence (see [4]). When $d = 0$, the above becomes the classical ARMA stationary process. The $(1 - L)^d$ "preprocessing" term consists of d banks of incrementation operators $(1 - L)$, in case the raw sequence $\{y(k)\}$ appears nonstationary, but can be made stationary by incrementation. The Smallest CANonical (SCAN) correlation method and the Extended Sample Autocorrelation Function (ESACF) method are used to identify tentative orders $(p + d, q)$ of the stationary or the nonstationary models of the signals as $ARMA(p + d, q)$. Should the SCAN and ESACF methods indicate that $p + d \geq 1$, then the Augmented Dickey-Fuller (ADF) unit root test should be used to determine whether the term of degree $(p + d)$ is a purely autoregressive term or whether it has a unit root. In the former case where the unit root test fails, we set $d = 0$ and we have an ARMA model. In the latter case where the unit root test passes, we go to the incremental signal $(1 - L)y$ and reapply the Dickey-Fuller unit root test. This process is iterated until the unit root test fails. This yields d, with which the SCAN and ESACF methods are used on $(1 - L)^d y$ to derive the tentative degrees (p, q), which in turn yield tentative

polynomials AR_p and MA_q, and final selection is made on the basis of best possible least squares fit.

3.2 ARIMA modeling at various levels in various positions

For each of the 12 segments identified in Section 2 (Table 1), an $ARIMA$ model representative of that segment was derived as follows: Each segment was decomposed into subsegments of 5,000 points each and, for each subsegment, the auto correlation sequence $a_k : k = 1, ..., 25$ and the partial correlation sequence $b_k : k = 1, ..., 25$ for a lag of 25 were derived. Each subsegment defined a point $(\sum_{k=1}^{25} |a_k|, \sum_{k=1}^{25} |b_k|)$ in $\mathbb{R}^2$ and as such each segment led to a cluster in $\mathbb{R}^2$. By visual inspection, one such subsegment point was chosen at the middle of the cluster as representative of the segment. This led to 12 subsegments of 5,000 data points, each subsegment representative of a given segment. For each sample subsegment, the SCAN and ESACF methods indicated that $p + d \geq 1$ and the Augmented Dickey-Fuller unit root test indicated that this term had a unit root. Upon going to the first order difference signal $x(k) = y(k) - y(k-1)$, the Augmented Dickey-Fuller unit root test failed, so that y is a nonstationary signal with one unit root, that is, $d = 1$. In all cases, *only one* differentiation was necessary for the unit root test to fail. This led to 12 $ARIMA(p, d = 1, q)$ baseline models, labeled as the segments (see Table 1). These models are listed in the Appendix.

With these models at hand, we will examine how specific they are to the various levels and the various positions (see Figure 4). Another relevant issue will be to examine how accurate they are in their ability to predict the sEMG signal at the various levels (see Figure 3). This would provide some mathematically objective confirmation of the levels of care.

3.3 burst versus background signal

Visual inspection of the incremental sEMG signal of Figure 1, confirmed by more objective dynamic analysis [7], reveals that the sEMG signal can be decomposed into two dissimilar signals. The first one is associated with some "background" signal (see Figure 1) and the other one is associated with the "bursty" part of the signal. The autocorrelation and partial correlation functions are the tools that were used in [7] to discriminate the "burst" signal from the "background" signal. Roughly speaking, the burst signal is distinguished from the background signal as being more stationary as revealed by a faster decaying autocorrelation.

A rather surprising fact is that the discrimination between the "burst" part and the "background" part of the signal does not quite coincide with the intuitive, naked eye analysis of the raw sEMG signal classifying as "bursty" an area of accrued sEMG activity. However, the same intuitive, naked eye analysis applied to the *incremental signal* yielded results somewhat more consistent with the rigorous mathe-
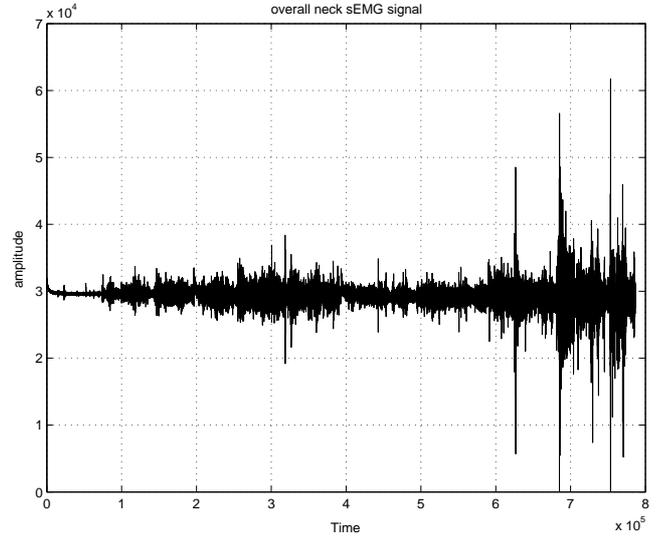

Figure 1: The overall raw sEMG signal recorded at the neck level showing at the beginning a "background" area and then becoming predominantly "bursty."

matical analysis.

Visual observation of the sEMG waveform sometimes allows for Levels 1,2,3 classification, in the sense that at high level of care the bursts become more intense and more frequent. If we attempt a more objective classification by dynamic modeling as it is proposed here, we would be forced to make a subjective choice between the backgound part or the burst part of the signal, and in case of the latter yet another choice would be *which* burst to choose. For these reasons, the approach taken here is to decompose the given segment of sEMG data record into several subsegments of equal length and choose the most relevant subsegment by clustering analysis. In other words, we leave it to the software to decide whether the dynamics is "background dominated" or "burst dominated." It turns out that only the first segment was "background" dominated while all other segments were "burst" dominated.

4 Model accuracy versus level of care

Regarding the quality of the models, that is, the ability of the models to predict the data at the corresponding level of care, we devised the following experiment: Each model was used as a one-step predictor on the data segment it was derived from. For each such data segment, the relative fitting error, that is, the average mean square one-step prediction error devided by the signal variance, was computed. The plot of the relative prediction error $E(i)$ versus the model index i is shown in Figure 2. This plot is decreasing, except for Models 7,8,9. Now, remember that around Models 7,8,9, there is a level trend reversal. The patient was already at Level 3 in Models 4,5,6 and then, because of the change of position, was brought back to Level 2 at Models 7,8,9. For this reason, we introduce the following permutation:

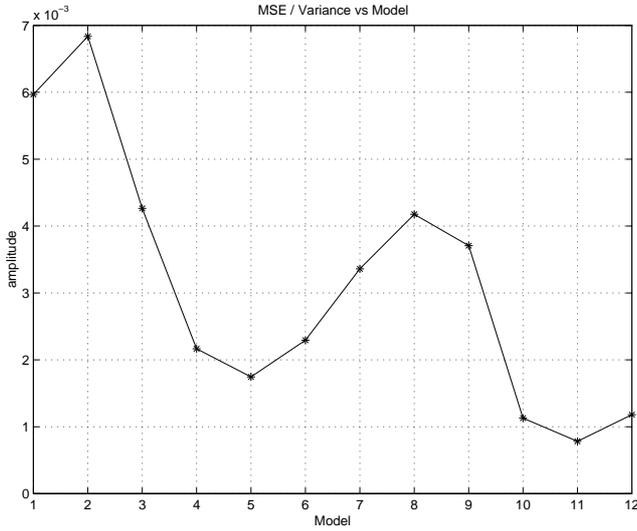$$P : (1, 2, 3, 4, 5, 6, 7, 8, 9, 10, 11, 12) \longrightarrow (1, 2, 3, 7, 8, 9, 4, 5, 6, 10, 11, 12)$$

Figure 2: Relative one step prediction error E versus model.
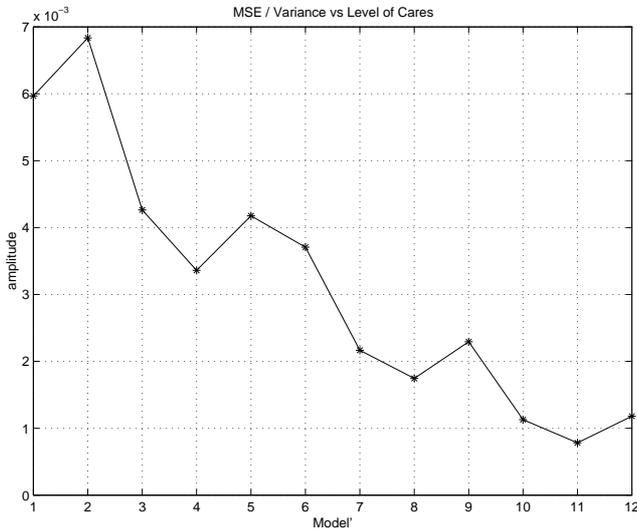

Figure 3: Relative one step prediction error $E \circ P$ versus level of care.

In other words, if we follow the right-hand side sequence, the patient starts at Level 1 in the prone position, then goes to Level 2/prone position, to Level 2/sitting, to Level 3/prone, and finally to Level 3/supine. This represents a monotone trend to higher and higher level of care. Call this model re-indexed consistently with the level of care $Model'$. Then upon plotting $E \circ P$ versus the index of $Model'$, which represents the level of care, the curve has an overall monotone decreasing appearance (see Figure 3). *It transpires from this that, as the patient goes from Level 1 to Level 2 to Level 3, the sEMG signal becomes, more predictable, more amenable to dynamical modeling.*

5 Level specificity and switching dynamics

Now, we try all 12 models on the *long range* data record. Of course, a model will fit the data segment from which it was identified; however, the same model may or may not fit the other data segments. In the latter case, we would conclude that there is some *"specificity"* in the model attached to a level of care.

The 4 neck recordings were concatenated to produce a single global recording of 786,432 data points. For each such data point $k \in \{1, 2, ..., 786432\}$, the interval $[k - 500, k]$ was considered and the model best fitting the data $F(k) \in \{1, 2, ..., 12\}$ was derived. The fitting criterion was based on the following mean square error:

$$\sum_{i=1}^{25} \left((a_i^{model} - a_i^{signal})^2 + (b_i^{model} - b_i^{signal})^2 \right)$$

where $\{a_i\}$ is the autocorrelation sequence and $\{b_i\}$ the partial correlation sequence of the incremental signal.

The results are plotted in Figure 4 in the form of a function

$$F : \{1, 2, ..., 786432\} \rightarrow \{1, 2, ..., 12\} \, .$$

The abscissa represents the 786432 data points. The ordinate represents the various models. For each k, $F(k)$ is the model that best fit the data segment. The crucial point is to observe that this function is nearly staircase shaped, *indicating a good correlation between the model and the level of care.* More specifically, the following features are worth mentioning:

1. Level 1, prone position, yields a most diffentiated signal because its model, 1, does not fit any data other than the early Level 1 data.

2. Level 2, prone, appears to follow models 2, 3. Level 3, prone, appears to follow models 4, 5, 6. However, Level 3 data, prone, also seems to be fitted by model 2 and to a lesser extend by model 4. Therefore, while Model 2-6 are specific to Level 2, prone and Level 3 prone, there are some difficulties at differentiating Level 2 from Level 3 in this position.

3. Level 2, sitting, yields a very differentiated signal since models 7-9 are the only ones capable of fitting this data.

4. Level 3, supine, also yields a very differentiated signal, because only models 10-12 fit the data, while these models do not fit other data.

The best fitting criterion yields an overall sEMG signal that can be represented, over a short period of time, by a selected ARIMA model and, over a longer period of time, by
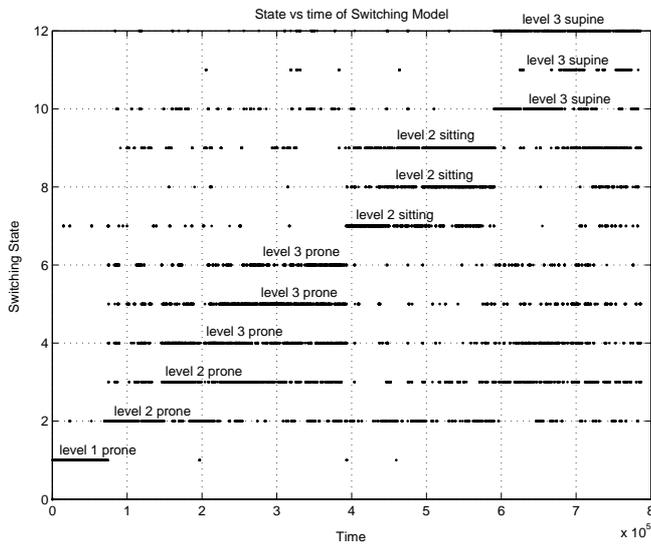
Figure 4: Best fitting model versus time.

Figure 5: Transition between Level 2 (Model 3) to Level 3 (Model 4).

switchings among the 12 models. These switchings represent transitions among the 3 levels of care, transitions between sitting, prone, and supine positions, etc. For purpose of illustration, we choose the transition between level 2 and level 3 (prone position), where we switch from model 3 to model 4. This is shown in Figure 5.

6 Conclusions

The main point of this paper is that the ARIMA models of the sEMG signals recorded during NSA entrainment appear to have some Level specificity (as Figure 4 indicates) and, more decisively, the predictability of the sEMG signal improves with the Level of care (as Figure 3 indicates). As such, some objective classification of the Levels of NSA by sEMG signal analysis can be anticipated in a foreseeable future.

The observation that the sEMG signal becomes more deterministic at higher Levels of care can probably be justified by a Hebbian learning argument. That is, at Level 3, the synaptic strengths are adjusted, the neural pathways are established, and consequently the signal becomes less random. The fact that the sEMG signal consists of a "background" part and a "burst" part is reminscent of single neuron bursting [5] and switching phenomena between different dynamical behaviors in many neurons dynamics [6]. However, such well-documented switchings as the gamma-beta and spindling-delta involve transition between rhythms of different frequencies [6] whereas in the NSA sEMG data there is no such frequency shift. It is of interest that the thalamus is known to have burst activity. However, it is not currently known if the thalamus is involved in the NSA physiological phenomena. However, functional MRI study did indicate that NSA has its neural pathways not limited to the spine
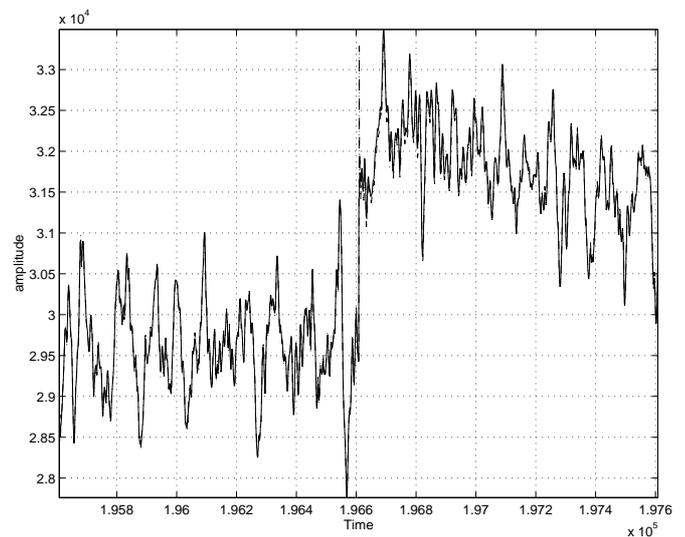
but involving some areas of the brain. On another tone, probably the most interesting challenge for control-theorists would be to figure out whether the dynamics of the sEMG signals could lead to some better understanding of the dural attachment feedback.

References

[1] S. Bohacek and E. A. Jonckheere. Chaotic modeling in network spinal analysis: Preliminary report: Nonlinear canonical correlation with alternating conditional expectation (ACE). *Journal of Vertebral Subluxation Research*, 2(4):188–195, December 1998.

[2] A. Breig. *Adverse Mechanical Tension in the Central Nervous System*. John Wiley and Sons, New York, 1987.

[3] Alf Breig. *Skull Traction and Cervical Cord Injury: A New Approach to Improved Rehabilitation*. Springer Verlag, 1989. ISBN: 0387504141.

[4] James D. Hamilton. *Time Series Analysis*. Princeton University Press, Princeton, New Jersey, 1994.

[5] Christof Koch. *Biophysics of Computation: Information Processing in Single Neurons*. Oxford University Press, New York, New York, 1999. ISBN 0-19-510491-9.

[6] N. Kopell. We got rythm: Dynamical systems of the nervous system. *Notice of the AMS*, 47(1):6–16, January 2000.

[7] P. Lohsoonthorn and E. Jonckheere. Nonlinear switching dynamics in surface electromyography of the spine. In *Conference on Physics and Control*, St. Petersbourg, Russia, 2003. submitted.

[8] J. W. McDonald, D. Becker, C. Sadowsky, J. A. Jane, T. E. Conturo, and L. Schultz. Late recovery following spinal cord injury. *J. Neurosurg (Spine 2)*, 97:252–265, 2002.

[9]   M. Panjabi. The stabilizing system of the spine. part i. function, dysfunction, adaptation, and enhancement. *Journal of Spinal Disorders*, 5(4):383–389, 1992.

Appendix: ARIMA Models

The dynamics models are of the ARIMA form of Equation 1. Here below, we list the $MA_q(L)/\left((1-L)^d AR_p(L)\right)$ parts of Model 1 through Model 12, successively.

$$\frac{\left(1.0000 + 0.0773L + 0.6378L^2 - 0.1316L^3 - 0.2238L^4 - 0.6875L^5 - 0.2600L^6 - 0.1456L^7 - 0.2506L^8\right)}{\left(1.0000 + 0.0372L + 0.5072L^2 - 0.3228L^3 - 0.2594L^4 - 0.6970L^5\right)}$$

$$\frac{\left(1.0000 - 1.5278L + 1.3171L^2 - 1.5720L^3 + 1.1330L^4 - 1.2295L^5 + 1.3809L^6 - 0.9696L^7 + 0.5316L^8 - 0.0509L^9 - 0.0119L^{10}\right)}{\left(1.0000 - 2.4427L + 2.5659L^2 - 2.2503L^3 + 2.0249L^4 - 1.7460L^5 + 2.0133L^6 - 2.1382L^7 + 1.2847L^8 - 0.3078L^9\right)}$$

$$\frac{\left(1.0000 - 0.0245L - 0.4241L^2 - 0.2811L^3 - 0.5598L^4 - 0.1522L^5 - 0.1382L^6 + 0.0705L^7 + 0.1951L^8 + 0.1683L^9 + 0.1515L^{10}\right)}{\left(1.0000 - 1.1864L - 0.3999L^2 + 0.6034L^3\right)}$$

$$\frac{\left(1.0000 + 1.4416L + 0.7228L^2 + 0.4781L^3 - 0.2483L^4 - 1.2198L^5 - 0.9782L^6 - 0.4457L^7 - 0.4075L^8 - 0.3069L^9\right)}{\left(1.0000 + 0.2650L - 1.0099L^2 - 0.0288L^3 - 0.0417L^4 - 0.6139L^5 + 0.5552L^6 + 0.6168L^7 - 0.5576L^8 - 0.3017L^9 + 0.3214L^{10}\right)}$$

$$\frac{\left(1.0000 + 0.5872L - 0.1654L^2 - 0.0872L^3 - 0.2493L^4 - 0.8460L^5 - 0.2278L^6\right)}{\left(1.0000 - 0.5541L - 0.9865L^2 + 0.4775L^3 + 0.2997L^4 - 0.6276L^5 + 0.7146L^6 + 0.1827L^7 - 0.5764L^8 - 0.0713L^9 + 0.2444L^{10}\right)}$$

$$\frac{\left(1.0000 - 1.0173L + 0.3279L^2 - 0.3778L^3 - 0.1436L^4 - 0.0668L^5 - 0.1309L^6 + 0.3163L^7 - 0.0501L^8 + 0.1239L^9 + 0.0191L^{10}\right)}{\left(1.0000 - 2.1721L + 1.4307L^2 - 0.2568L^3\right)}$$

$$\frac{\left(1.0000 - 0.4658L + 0.3745L^2 + 0.6391L^3 - 0.8152L^4 + 0.1723L^5 - 0.3149L^6 - 0.3524L^7 - 0.0108L^8 - 0.2247L^9\right)}{\left(1.0000 - 1.2814L + 0.4845L^2 + 0.6322L^3 - 1.1610L^4 + 0.4930L^5\right)}$$

$$\frac{\left(1.0000 + 1.3303L + 0.6434L^2 - 0.1922L^3 - 1.1233L^4 - 0.8024L^5 - 0.5017L^6 - 0.3430L^7\right)}{\left(1.0000 + 0.2693L - 0.9152L^2 - 0.7401L^3 - 0.2618L^4 + 0.8768L^5 + 0.2539L^6 - 0.3473L^7\right)}$$

$$\frac{\left(1.0000 + 1.2300L + 1.0099L^2 + 0.2572L^3 - 0.7867L^4 - 0.7440L^5 - 0.9869L^6 - 0.6494L^7 - 0.2892L^8 - 0.1165L^9 + 0.0834L^{10}\right)}{\left(1.0000 + 0.0976L - 0.4730L^2 - 0.6680L^3 - 0.4451L^4 + 0.6219L^5\right)}$$

$$\frac{\left(1.0000 + 1.5170L + 1.5186L^2 + 0.6106L^3 - 0.5117L^4 - 1.0981L^5 - 1.1221L^6 - 1.1082L^7 - 0.5011L^8 - 0.2557L^9\right)}{\left(1.0000 + 0.1900L - 0.5753L^2 - 0.6809L^3 - 0.1212L^4 + 0.5036L^5 + 0.3910L^6 - 0.4960L^7 + 0.0627L^8\right)}$$

$$\frac{\left(1.0000 + 1.8439L + 1.1903L^2 + 0.8994L^3 + 1.0293L^4 + 1.1281L^5 + 1.3393L^6 + 1.1731L^7 + 0.9236L^8 + 0.5660L^9 + 0.1515L^{10}\right)}{\left(1.0000 + 0.0080L - 1.2682L^2 + 0.7813L^3 + 0.8045L^4 - 0.3462L^5\right)}$$

$$\frac{\left(1.0000 + 0.1109L + 0.0696L^2 - 0.1057L^3 - 0.3819L^4 + 0.1525L^5 - 0.1356L^6 - 0.1927L^7 - 0.1778L^8 - 0.0660L^9 - 0.2658L^{10}\right)}{\left(1.0000 - 1.2267L + 0.0330L^2 + 0.2253L^3 + 0.0688L^4 + 0.5411L^5 - 0.8015L^6 - 0.0046L^7 + 0.2027L^8 + 0.1045L^9 - 0.0934L^{10}\right)}$$